



Article

Anticipating the Collapse of Urban Infrastructure: A Methodology Based on Earth Observation and MT-InSAR

Ignacio Rodríguez-Antuñaño , Joaquín Martínez-Sánchez, Manuel Cabaleiro and Belén Riveiro *

CINTECX, Universidade de Vigo, GeoTECH Group, Campus Universitario de Vigo, As Lagoas, Marcosende, 36310 Vigo, Spain; ignacio.rodriguez.antunano@uvigo.gal (I.R.-A.); joaquin.martinez@uvigo.gal (J.M.-S.); mcabaleiro@uvigo.gal (M.C.)

* Correspondence: belenriveiro@uvigo.gal

Abstract: Large-scale infrastructure monitoring and vulnerability assessment are crucial for the preservation and maintenance of built environments. To ensure the safety of urban infrastructure against natural and man-made disasters, constant monitoring is crucial. To do so, satellite Earth observation (EO) is being proposed, particularly radar-based imaging, because it allows large-scale constant monitoring since radar signals are not blocked by clouds and can be collected during both day and night. The proposed methodology for large-scale infrastructure monitoring and vulnerability assessment is based on MT-InSAR time series analysis. The homogeneity of the year-to-year displacement trend between each point and its surrounding points is evaluated to determine whether the area is a stable or vulnerable zone. To validate the methodology, four case studies of recently collapsed infrastructures are analyzed. The results indicate the potential of the proposed methodology for predicting and preventing structural collapses.

Keywords: satellite monitoring; collapse; Line 12 of the Mexico City Metro; Capriogliola bridge; Font Nova urbanization (Peñíscola); Champlain Towers South (Miami)



Citation: Rodríguez-Antuñaño, I.; Martínez-Sánchez, J.; Cabaleiro, M.; Riveiro, B. Anticipating the Collapse of Urban Infrastructure: A Methodology Based on Earth Observation and MT-InSAR. *Remote Sens.* **2023**, *15*, 3867. <https://doi.org/10.3390/rs15153867>

Academic Editors: Songhan Zhang, Guangdong Zhou and Jian Li

Received: 30 June 2023

Revised: 28 July 2023

Accepted: 2 August 2023

Published: 4 August 2023



Copyright: © 2023 by the authors. Licensee MDPI, Basel, Switzerland. This article is an open access article distributed under the terms and conditions of the Creative Commons Attribution (CC BY) license (<https://creativecommons.org/licenses/by/4.0/>).

1. Introduction

One of the major challenges of our society is the preservation and maintenance of the built environment, not only because of its financial value, but, most importantly, because of the safety and serviceability of constructions. Indeed, safety is one of the main concerns of structural design; hence, regulations have been developed by experts and public administrations that are focused on the design and construction of structures with the maximum safety level. However, no countries have implemented regulations or standards for the structural evaluation of in-service infrastructure, thus ignoring the deterioration and structural modifications that may arise during the life cycle of the infrastructure, as well as the change in the conditions since they were designed and built [1,2].

Being aware of the increasing number of extreme events, mainly natural (where climate change plays an important role), but also man-made (accidents, negligence, vandalism, or terrorism), concrete actions to improve the resilience of transportation infrastructure to these events are required. Therefore, it is important to take into consideration new meteorological conditions, loading and usage conditions, and changes in the behavior of the population in order to evaluate whether the infrastructure is operating in safe conditions. An example of the effort to analyze the long-term relationships between urban development and the emerging subsurface environmental problem is the analysis of land subsidence and the comparison of the differences and commonalities across Asian developing countries using a stage model [3]. However, considering the huge number and dispersion of infrastructure assets and buildings subjected to the potential actions of extreme events, new solutions are required to monitor and evaluate in-service structures on a large scale, as well as to prioritize detailed studies on those structures affected by

a larger vulnerability. This approach includes, for instance, the creation of a risk index system composed of hazardous conditions and vulnerability of land subsidence in the Shanghai region, and the subsequent establishment of a risk assessment model [4]. Another approach is the analysis of hypsometric changes in urban areas resulting from multiple years of human activity to evaluate risk areas [5].

Satellite Earth Observation (EO) is being proposed as a suitable technology for large-scale land cover monitoring. Among the available data from these satellite sensors, radar-based imaging has been proposed for those phenomena related to terrain displacement. One of the main limitations for optical satellite remote sensing systems is related to the effect of clouds, which may prevent the adequate observation of the target area of study. The wavelength of radar systems complements the use of optical images because the signal is not blocked by clouds and, because radar systems are active sensors, they support data collection during both day and night. In addition, Synthetic Aperture Radar (SAR) systems permit the analysis of interferometric data based on several methods that evolved over the years from the original differential interferometric SAR (DInSAR), based on the processing of two images, to the present MultiTemporal InSAR (MT-InSAR), which uses a higher number of images to improve the precision of the method [6]. For example, using DInSAR in the Upper Silesian coal basin in southern Poland, the subsidence of the ground of numerous cities due to intensive underground coal exploitation was detected [7,8].

Radar satellite platforms cover both commercial and public missions, which share the images free of cost. Examples of commercial radar satellites include TanDEM-X, RadarSat-2, COSMO-SkyMed, ALOS-2, SEOSAR/PAZ, SAOCOM, and RCM, which are widely utilized for infrastructure monitoring because their high resolution [9]. For instance, a study focused on ground motion monitoring in New Delhi compared the impact of SAR resolution and wavelengths from multiple sensors, such as Cosmo-SkyMed, Sentinel-1A-B, and ALOS PALSAR [10]. Additionally, another paper conducted a comparative analysis of Radarsat-2, Envisat, and TerraSAR-X satellites for line-infrastructure monitoring, presenting performance assessment metrics [11]. Regarding public missions, Copernicus' Sentinel-1 is a frequently used alternative for radar EO because of its worldwide coverage and free image availability. In addition, it is possible to monitor movements on the surface of the Earth through Free and Open-Source Software (FOSS) [12].

Focusing on the built environment, radar MT-InSAR, which was developed by Alessandro Ferretti in 2000 [13], is a proven method for the evaluation of potential damage in infrastructure assets. For example, urban subsidence has been addressed in a study performed in the metropolitan area of Rome [14], where the authors are among the pioneers of the use of Copernicus Sentinel-1 data and FOSS for infrastructure monitoring in the city using MT-InSAR. Another example of the initial experiences of detecting infrastructure problems through urban monitoring consists of identifying buildings with cracks using ENVISAT images and SARPROZ software [15]. Moreover, the first national satellite-based railway monitoring system was achieved using images between 2010 and 2015 of Radarsat-2 through the InSAR technique [16]. One of the first works on infrastructure collapse was the analysis (of the Hintze Ribeiro bridge) through ERS SAR images covering the Entre-os-Rios area [17]; the work related high values to the possibility of collapse. Despite the numerous works proposing InSAR for large-scale monitoring of infrastructure, very few works have focused on predictive assessment in order to, for instance, anticipate a structural collapse. Among the works in this last group are the use of a filter with a trend change detection algorithm to highlight areas of significant deformation [18]. Other examples are the automatic identification at the regional scale of trend variations within a single and continuous Mt-InSAR analysis by incorporating recent images [19]; the systematic and regular analysis of images to identify any changes in the deformation pattern and highlight anomalous points [20]; the combination of a multiple interferometric approach with a time series data mining algorithm designed to recognize points with significant trend variations [21]; the search for anomalies in the persistent scatterer deformations in the spatial and temporal dimensions [22]; and the identification and monitoring in wide

areas, and the discretization of the most critical deformations to create alerts [23]. Another work located potential unstable or dangerous regions using the spatial velocity gradation and the temporal evolution trend of surface displacements in large-scale areas [24]. A procedure was also developed with the aim of semi-automatically identifying clusters of active persistent scatterers and preliminarily associating them with different potential types of deformational processes over wide areas [25]. A risk map was also created at the municipal level by evaluating the risk subcomponents: danger, intensity, and vulnerability [26].

In summary, some methods use a single and classic Mt-InSAR analysis to assess whether there is a significant increase in the terrain movement through its displacement trend, and then to launch an alert [18–21]. Other methods use a cluster of points with a common tendency of instability to locate vulnerable zones in infrastructure or for risk management at a large scale [22–26]. However, our novel approach compares the Mt-InSAR analysis year by year to identify areas with high variance values, and thereby locate vulnerable areas, rather than via a complete single analysis of the time series.

Moreover, a shortcoming of the aforementioned approaches consists of the lack of an application to areas where a structural collapse actually happens, making it difficult to evaluate these methodologies in real cases. This work solves this issue through the analysis of several real cases of collapse by applying accessible predictive monitoring using FOSS.

In this paper, we propose a new method for large-scale infrastructure monitoring and vulnerability assessment using MT-InSAR time series analysis. For this purpose, the novelty of our approach consists of evaluating the homogeneity of the year-to-year displacement trend between each point and the surrounding points. When a point follows the same displacement trend as that of the surrounding points, it is classified as a stable zone; however, if there is a significant difference between the point and its neighbors, it is classified as a vulnerable zone. To validate the methodology, four case studies, in which various types of constructions subjected to different environmental conditions had recently collapsed, are analyzed.

The structure of the paper is as follows: in Section 2, the proposed methodology is explained. Section 3 includes the description of the different case studies and the corresponding data processing. In Section 4, the results are analyzed, and these are later discussed in Section 5. Finally, Section 6 summarizes the main conclusions of the work.

2. Methodology

In order to achieve the goal explained above, our methodology is built in three main phases as depicted in Figure 1: (1) interferogram generation and stacking using the software SNAP; (2) computation of the persistent scatterers (PSs) using StaMPS software; (3) and data analysis and detection of vulnerable areas using QGIS v3.32.1 software.

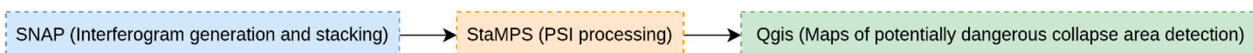


Figure 1. Methodology used in this work.

2.1. Obtaining the LOS Map and Generation of Interferograms

Synthetic Aperture Radar Interferometry (InSAR) is an active remote sensing technique based on the measurement of the phase shift between two or more radar images of the same scene collected at different times. The analysis of these images allows the detection and parameterization of displacements of the observed object, or land in the case of space-borne radar antennas. In this last system configuration, the radar antenna emits an electromagnetic signal in the microwave band that interacts with the ground, and part of the signal is reflected back to the satellite. The backscattered signal is received and recorded by the onboard radar system and used to generate a SAR image. The SAR image consists of a 2D array where the azimuth coordinate is represented by the rows, the slant-range coordinate is given in columns, and the value of each cell unit is characterized by an amplitude and the phase information of the backscattered signal. The resultant image is the so-called LOS (line-of-sight) map.

Our methodology consists of dividing the processing by year, and therefore, the workflow for interferogram generation and stacking is depicted in Figure 2. Here, the first step consists of selecting the master image (in SLC format) for each year of the analysis. The master image will collate the rest of the images for each annual analysis in order to detect and monitor changes by comparison between the master image and other images at time t . This analysis is performed using the free ESA program of SNAP [27]. The analysis continues by using the snap2stamps tool [28], which supports the automation of the processing chain for interferograms and is compatible with StaMPS.

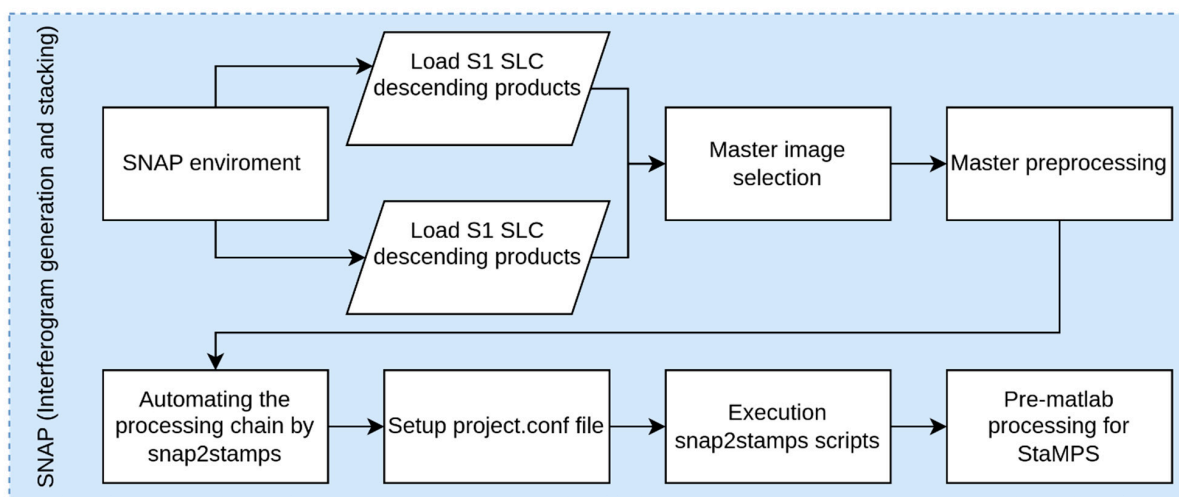


Figure 2. Workflow for the interferogram generation using Sentinel-1 images.

2.2. Extraction of Persistent Scatterers to Monitor Land Deformation

In our work, we use the Persistent Scatterer Interferometry (PSI) method [13], which is a method that allows identifying natural targets (reflectors) whose phase remains stable over time. To assess whether a point has a stable phase, an interferometric analysis is performed through the time series of the different images. Thus, a threshold between 0.25 and 0.40 is typically used when using Sentinel-1 images [6]. The higher the threshold, the larger the number of pixels (points) that results from the analysis; conversely, a more restrictive analysis will involve a lower value for the threshold. These resultant stable reflectors are called persistent scatterers (PSs), and typically belong to built objects such as buildings or civil structures. These PS points are defined through geographical coordinates and displacement data. A threshold of 0.65 was selected in our research, after performing our tests by heuristic methods. In these tests, the objective was to have a balanced threshold that does not make the temporal incoherence excessive, but, at the same time, is sufficient to obtain a good density of PS points covering urban infrastructure. In this way, sudden movements can be detected, which can be eventually related to future infrastructure structural failure.

The PS extraction was performed using StaMPS [29]. StaMPS is an open-source program for the Multi-temporal Interferometric Synthetic Aperture Radar (MT-InSAR) technique. The processing itself includes C++ programs and MATLAB scripts to identify coherent pixels and extract the warp signal for these pixels.

This analysis using StaMPS is implemented within MATLAB following the workflow depicted in Figure 3. This MATLAB code consists of sequential instructions or steps (commands) to obtain the PSs and the corresponding deformation map of the study area. Therefore, the sequence involves loading the data obtained from SNAP into the MATLAB environment to calculate temporal coherence by estimating the phase noise and the spatially uncorrelated DEM error (to remove the topographic phase component and geocode the results, we used the SRTM 1-arcsec DEM with 30 m resolution); thus, a first selection of PSs can be made so that those considered noisy can be eliminated. Then, the data are resampled

to drop pixel errors and merged to perform phase unwrapping. Finally, the results are filtered to remove the spatially correlated look angle errors and the noise from atmospheric disturbances. The correct PSs can then be exported with their velocity and time series trend.

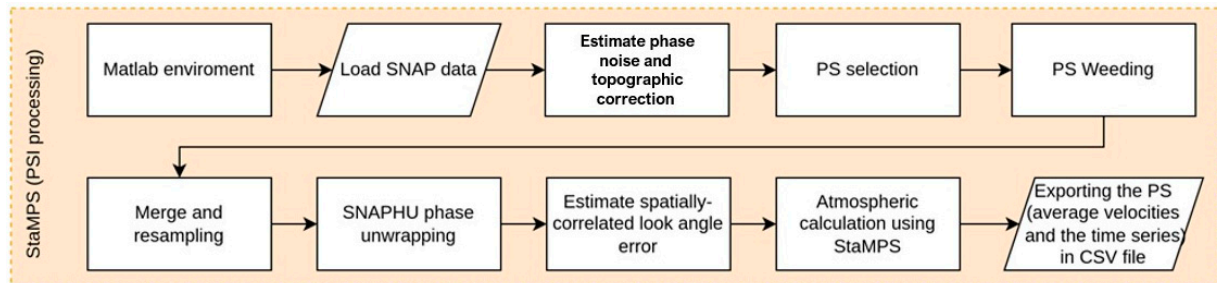


Figure 3. Workflow for PS extraction.

It is necessary to clarify that, in MT-InSAR processing, the Atmospheric Phase Screen (APS) plays a crucial role in the accurate estimation of the deformation values, as it allows us to remove the atmospheric phase perturbations from the interferometric measurements at the time of data acquisition, thus improving the accuracy of the final deformation results. This error is produced by delays in radar signals caused by variations in the Earth's atmosphere, particularly in the troposphere [29,30].

The execution of the aforementioned code in StaMPS requires the definition of various parameters [30] that must be evaluated for every study area. Table 1 summarizes the parameters set in the case studies presented in this paper. The values were set in accordance with the settings that allow the detection of subtle displacements in bridges.

Table 1. Parameter values adapted from [30] for the case studies presented in this paper.

Parameter	Default	Used
max_topo_err	20	10
filter_grid_size	50	40
clap_win	32	16
scla_deramp	'n'	'y'
percent_rand	20	1
unwrap_grid_size	200	50
unwrap_time_win	730	180
scn_time_win	365	180
scn_wavelength	100	50
unwrap_gold_n_win	32	16

Once the deformation map has been obtained, the different files generated are exported for further analysis, as explained in the forthcoming section.

2.3. PS Geospatial Analysis

One of the main novelties of our proposed methodology compared to other works using MT-InSAR is that, instead of using a continuous time series for the entire period under evaluation, we focus the analysis on each year for each orbit (ascending and descending), and then, for each pixel, we compare the evolution of the displacement trend among the different years. Thus, the temporal evolution trend (TET) is computed year by year as the cumulative sum of the absolute values of displacement during the year at every single point. Later, the final evolution trend (FET) is computed as the variance of the absolute values of the displacement for all years of the same pixel.

The objective is to analyze the final evolution trend (FET) and classify points into (i) stable zones if there are no significant differences in a year with regards to the others; or (ii) vulnerable zones when there is a significant change in the FET of consecutive years. The initial hypothesis is that these last points represent the areas where a sudden structural failure is prone to happen.

To proceed with the analysis, QGIS software was used according to the workflow presented in Figure 4. The first step is obtaining the TET for each point (PS) of the years analyzed. As the product obtained in the previous phase consists of a series of point clouds for each year and orbit, a common grid is defined in order to rasterize the data with a pixel size of 20 m. The choice of 20 m pixels is taken as the minimum resolution, and is obtained from the maximum resolution of Sentinel-1 images.

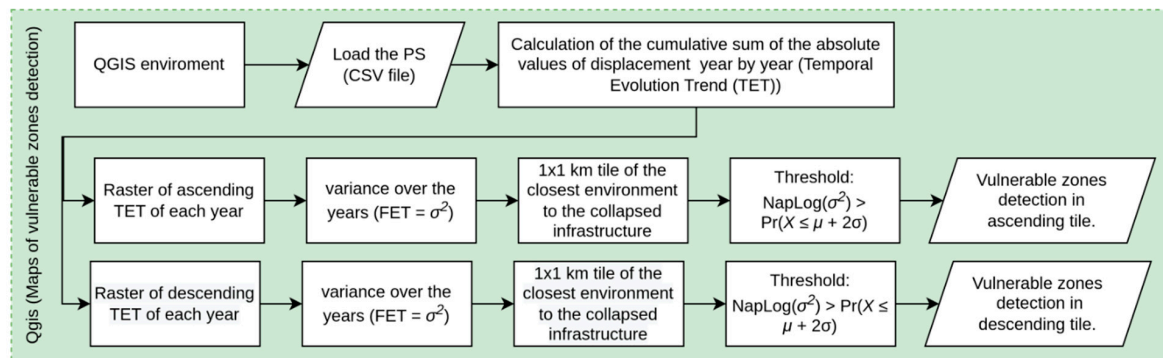


Figure 4. Workflow of the third step for each year of the analysis of Sentinel-1 images to detect areas potentially at risk of dangerous collapse.

The next step is to analyze how much the accumulated displacements (TET) vary over the years, to determine the variance that exists, resulting in the FET for the same pixel over the years, through the following formula:

$$\sigma^2 = (\sum (x_i - \mu)^2) / N, \tag{1}$$

where:

σ^2 is the variance obtained from the MT-InSAR results of each pixel over the years of the analysis, that is, the FET.

x_i is the absolute displacement of year i (TET).

μ is the mean of all absolute values of the annual displacement.

N is the number of years of the total analysis.

To avoid undesired effects due to the heterogeneity of land and to consider only the closest environment of each point, the study area is divided into 1×1 km tiles. This operation smooths the variance of the FET in the entire study area, and thus enhances the perception of potential vulnerable points.

Therefore, the vulnerable points for each of the orbits in its corresponding tile (following the Empirical Rule in Table 2) will always be those whose variance of FET exceeds the mean (μ) by 2 times the variance (σ) of the set of points of the tile. This means that, in a normal distribution, approximately 95% of the points will be classified as stable.

Table 2. Pixel classification criteria ¹.

Pixel Classification	Threshold
Stable areas	$\text{NapLog}(\sigma^2) < \Pr(\mu - 2\sigma \leq X \leq \mu + 2\sigma)$
Vulnerable areas	$\text{NapLog}(\sigma^2) < \Pr(X \leq \mu + 2\sigma)$

¹ Note: σ^2 represents the variance of the FET obtained from the MT-InSAR results of each pixel over the years of the analysis, NapLog is the logarithmic transformation in order to normalize the variance of FET, and X is an observation from a normally distributed random variable.

The Empirical Rule involves transforming the data into a normal distribution. The transformation carried out is logarithmic (NapLog) since the logarithmic transformation is useful for transforming distributions with a positive skew (because the histogram of the variance of the FET in each tile have a larger tail on the right); the left part will be expanded, while the right part will be compressed, meaning that the resulting curve fits better to a normal one.

3. Experiment and Data Processing

To demonstrate that this methodology is correct and effective, random case studies where structural collapses recently happened were selected.

Study Area and Data

Four study areas were selected to investigate whether it is possible to predict sudden collapses in urban areas where an actual collapse was experienced, as follows:

- Infrastructure located in areas of continuous subsidence. Mexico City has experienced multiple earthquakes and is located on top of a lagoon, which makes the area unstable. The specific infrastructure that was analyzed consists of the accident that occurred on 3 May 2021, on Line 12 of the Mexico City Metro. This accident may have been caused by the placement and welding of the bolts that connect the girders of the steel viaduct with the concrete slab [31].
- Infrastructure in semi-urban environments surrounded by vegetation, where two case studies were considered. The first infrastructure analyzed is the Caprigliola bridge (Italy), which collapsed over the Magra river on 8 April 2020. The causes of the collapse are still to be determined [32]. The second infrastructure analyzed consists of a building that partially collapsed in Peñíscola (Spain), on 25 August 2021 [33].
- Infrastructure in coastal environments. On 24 June 2021, the Champlain Towers South, a 12-story condominium located in the beachfront suburb of Surfside, Miami (United States), partially collapsed. The degradation of the reinforced concrete structural support, attributed to water penetration and corrosion of the reinforcing steel, is being studied as the focus of the causes for the collapse. This evidence was identified in 2018 and worsened by April 2021 [34]. Other contributing factors being considered include land subsidence, insufficient reinforcing steel, and corruption during construction [35,36]. The Surfside collapse is considered the third largest building failure in the history of the United States [37].

Available Sentinel-1 images were used to monitor the study areas by the time of their collapse. The acquisition time and properties of the used Sentinel-1 data are shown in Table 3.

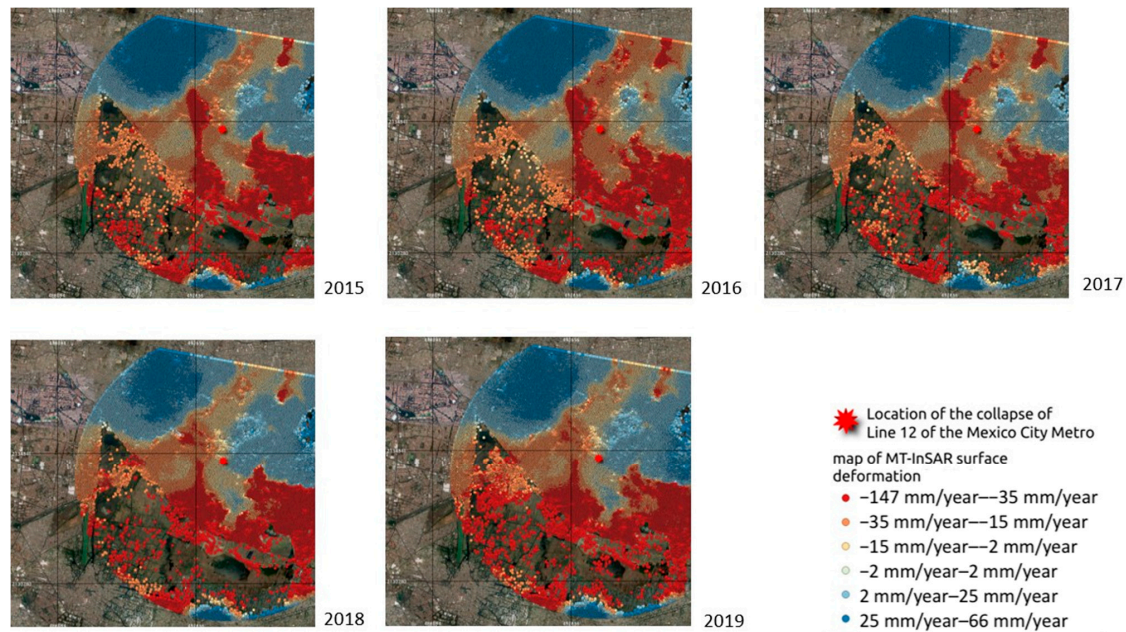
Table 3. Sentinel-1A/B datasets used, showing orbit path and image time period.

Case Study	Ascending 2	Descending 3
Line 12 of the Mexico City Metro	23 March 2015 to 2 May 2021	20 March 2015 to 29 April 2021
Caprigliola bridge	2 August 2015 to 7 April 2020	12 October 2015 to 6 April 2020
Building in the Font Nova urbanization (Peñíscola)	24 March 2015 to 12 May 2017	30 March 2015 to 13 March 2017
	and 4 October 2018 to 25 August 2021	and 4 October 2018 to 25 August 2021
Miami	9 October 2016 to 21 June 2021	No data

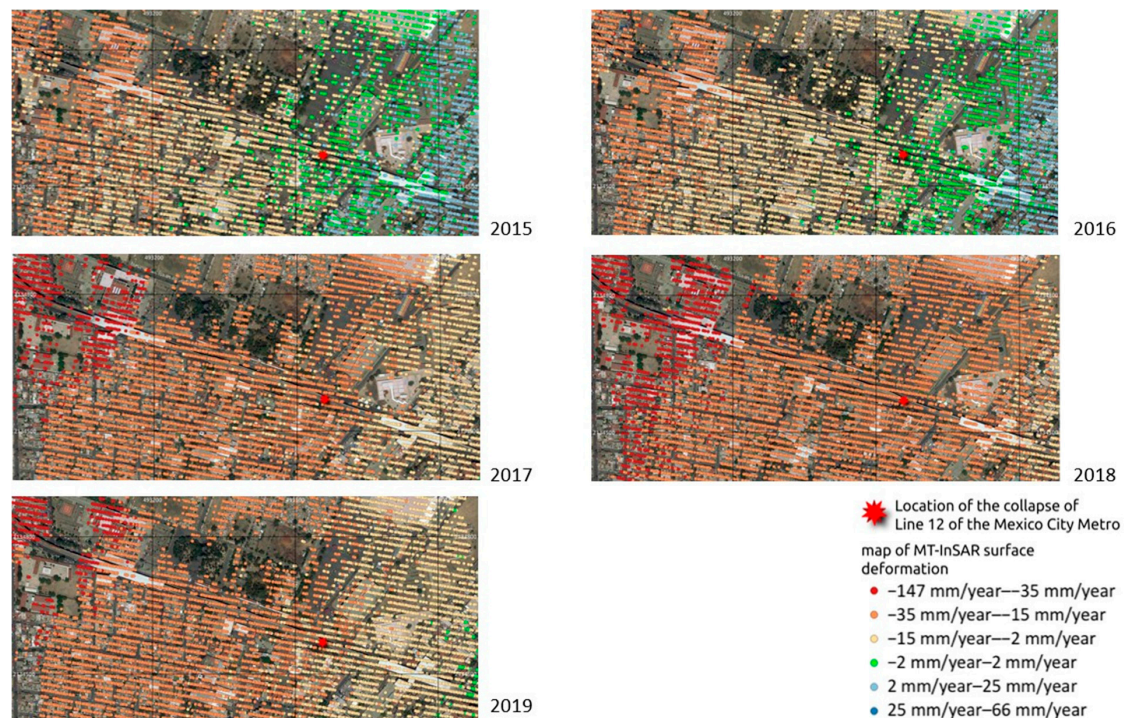
4. Results and Analysis

Even though the workflow was applied to all case studies, for simplicity, in this section, only the first case study is detailed as an example of the developed methodology. For the remaining case studies, only the final results are presented. Finding deformation patterns over time in an isolated manner in infrastructure is not easy, as shown for the first case

study (Line 12 of the Mexico City Metro) in Figure 5. Therefore, this new methodology is proposed through the FET map for each year (2015 to 2020). As mentioned in Section 2.3, the variance of the FET value for the same pixel over the years of analysis was calculated for both ascending images (in Figure 6) and descending images (in Figure 7).



(a)



(b)

Figure 5. (a) Map of MT-InSAR surface deformation (2015–2020) in descending images of the entire study area. (b) Detailed map of MT-InSAR surface deformation (2015–2020) in descending images in the specific infrastructure where the accident occurred on 3 May 2021 on Line 12 of the Mexico City Metro.

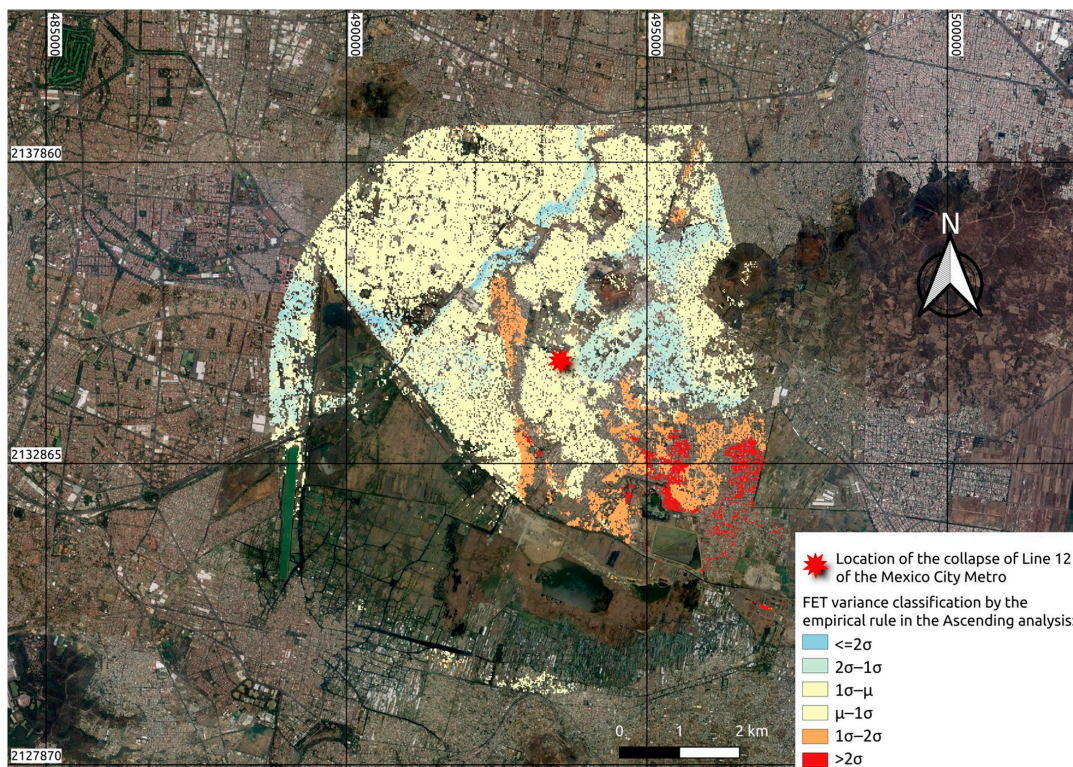


Figure 6. Variance obtained of the FET value for each pixel over the years of the analysis (2015–2020) in ascending images.

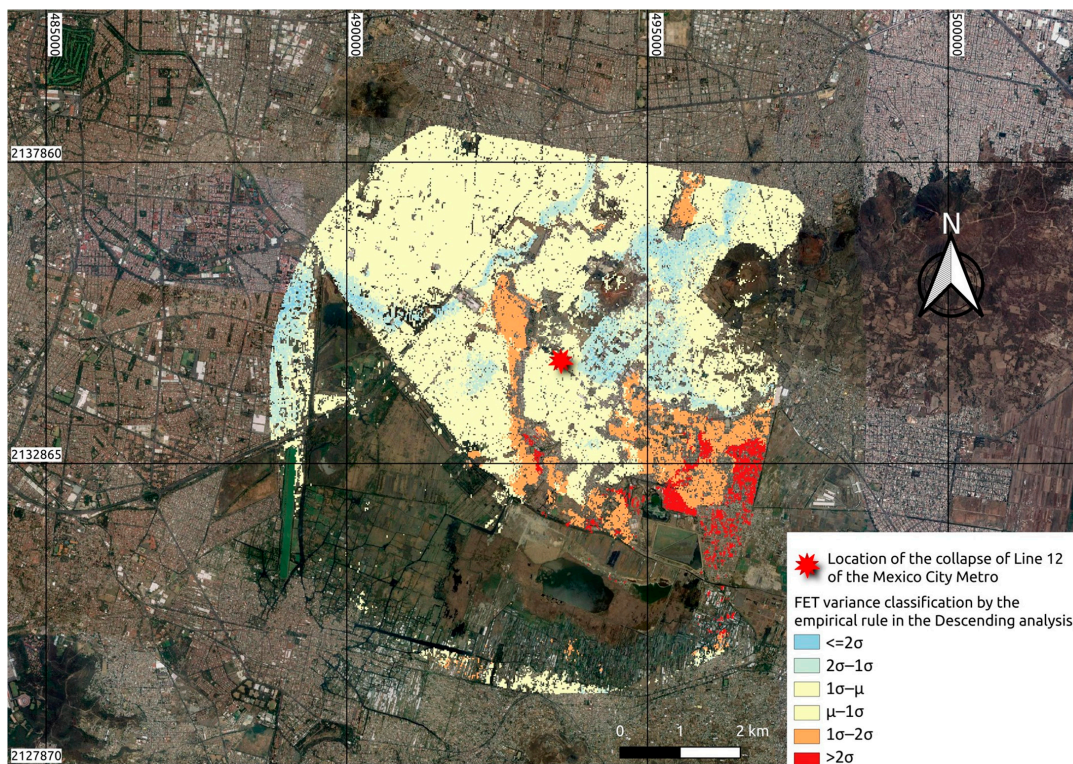


Figure 7. Variance obtained of the FET value for each pixel over the years of the analysis (2015–2020) in descending images.

The points of infrastructure collapse were located and are marked with a red point in Figures 8 and 9. The depicted variance in the 1 sq-km surrounding area provides an

indication of vulnerability, both for descending and ascending images. The values for this indicator are logarithmically transformed and filtered in the 2σ interval.

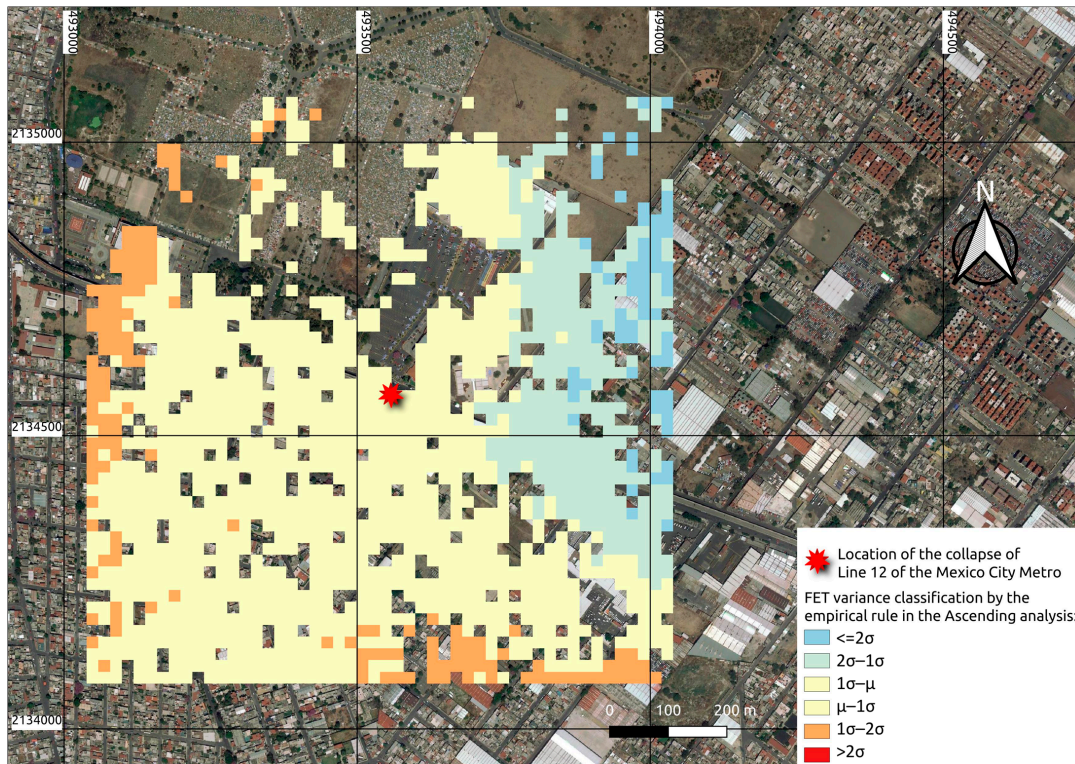


Figure 8. Variance obtained of the FET value for each pixel over the years of the analysis (2015–2020) in the 1×1 km tile in ascending images.

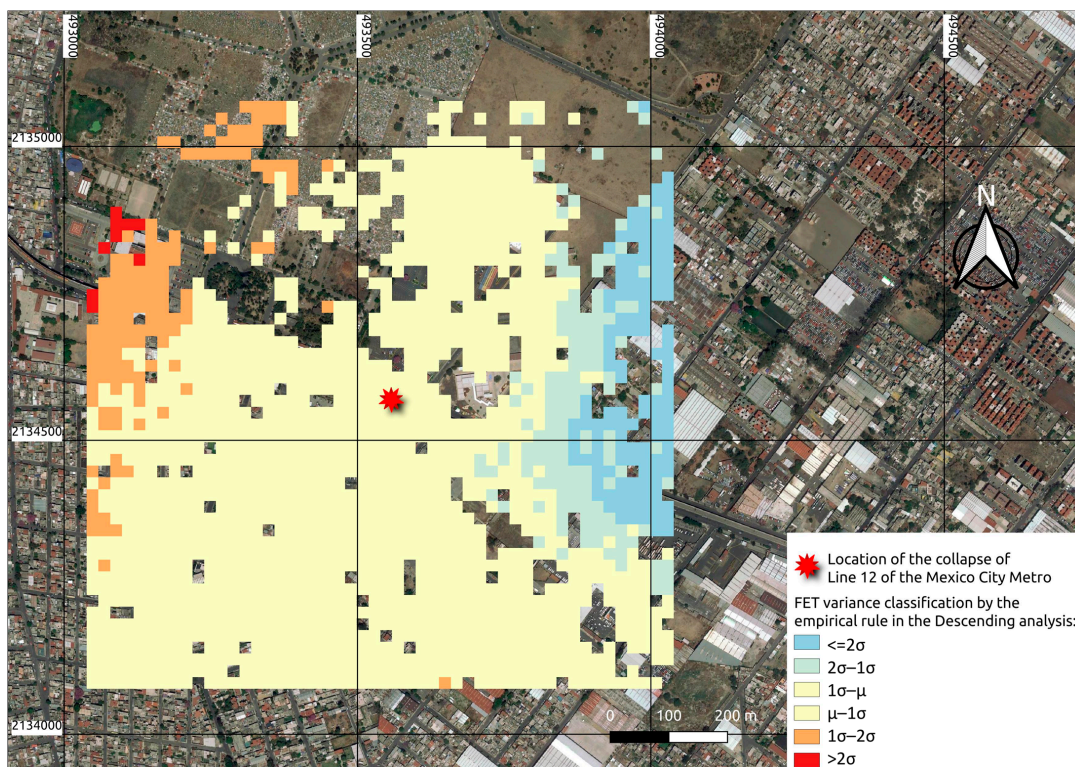


Figure 9. Variance obtained of the FET value for each pixel over the years of the analysis (2015–2020) in the 1×1 km tile in descending images.

Figure 10 shows that, in the descending case, the vulnerable zone, represented in magenta pixels, corresponds with one of the girders supporting the overpass that carries Line 12 of the Mexico City Metro near the Tezonco station. The vulnerable zone is defined as those pixels whose variance of FET exceeds the mean (μ) by 2 times the variance (σ) of the set of pixels of the tile.



Figure 10. The vulnerable zone, which concurs geographically with a girder that supported the overpass carrying Line 12 of the Mexico City Metro and that collapsed.

This shows how the methodology works for the early detection of vulnerable zones.

For the second case study, which is focused on the Caprigliola bridge, the variance of the FET map from 2016 to 2019 is obtained for both ascending and descending images. The analysis of the 1×1 km tile around the collapse location shows three vulnerable zones for the map with ascending images and two vulnerable zones for the map with descending images, as shown in Figure 11. In this case, only one of the areas is in close proximity to the collapsed bridge, showing the capability of the methodology to identify vulnerable zones, albeit only using ascending images.

For the third case study, due to a time gap in the available images, only the images from the same time intervals in both ascending and descending images were used, which limited the analysis to the years 2015–2016 and 2019–2021. The variance in the tile was logarithmically transformed and filtered using the criterion of $\Pr(X \leq \mu + 2\sigma)$, resulting in the identification of seven vulnerable zones in the ascending image map and eleven vulnerable zones in the descending image map, as shown in Figure 12.

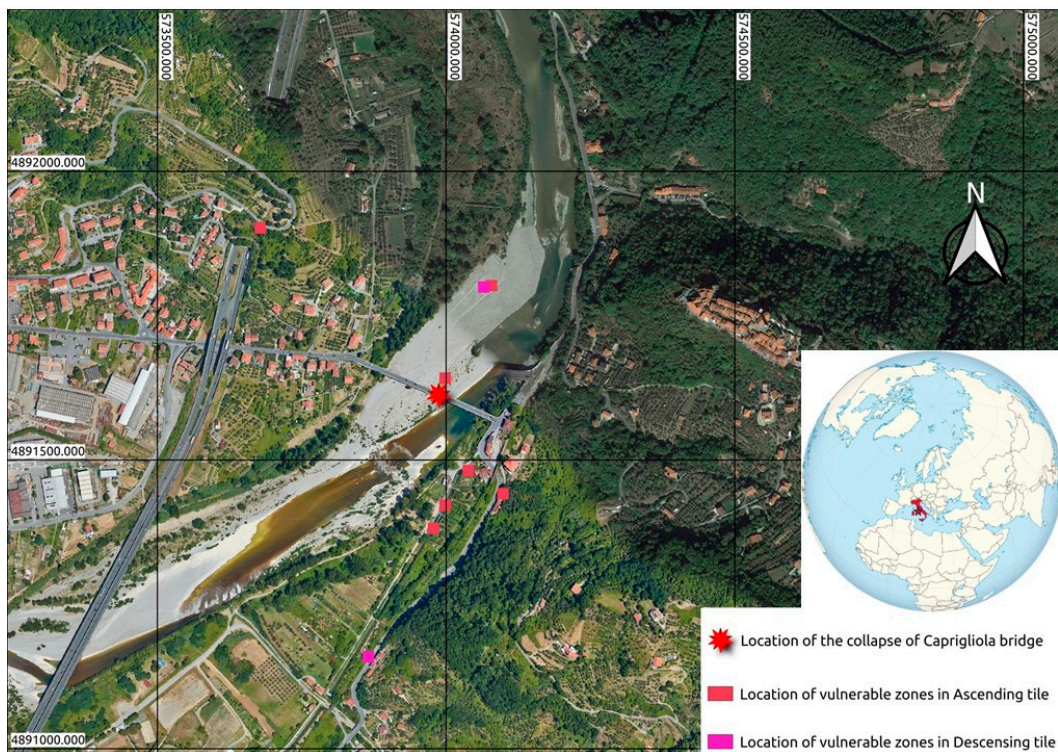


Figure 11. The vulnerable zone geographically concurs with the streambed of the Caprioliola bridge, which collapsed.

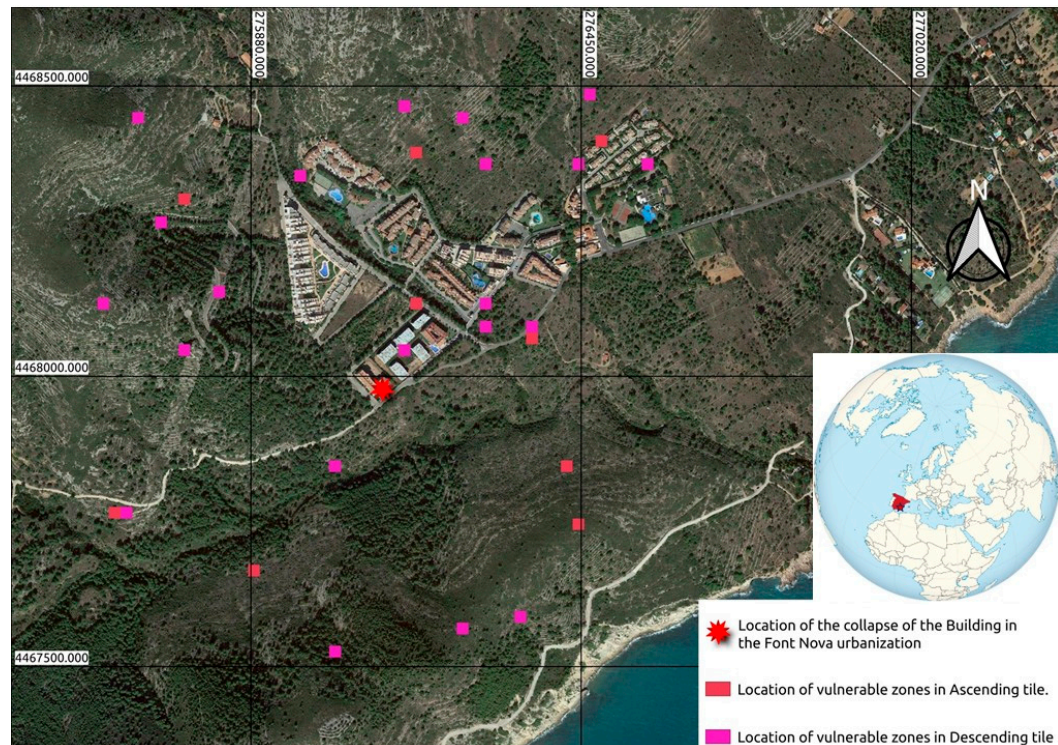


Figure 12. The vulnerable zone is geographically situated in the environment of the building, which collapsed, of the Font Nova urbanization.

In this case, only one of the identified areas is located close to the building where the collapse occurred. Despite the distance of approximately 65 m between the detected area and the building, it is still considered to belong to the building's environment based

on the resolution of Sentinel-1. Although there are more potential risk areas in this case study compared to the others, only five of them are located in built environments, with the others being false alarms caused by vegetation. The results were achieved only in the descending images.

In the final case study, which focuses on the collapse of Champlain Towers South, the variance of the FET map is obtained for the years 2017 to 2021, using only ascending images since they are the only images available for download. The results show six vulnerable zones in the map with ascending images, as shown in Figure 13. Of the six areas identified, only one coincides geographically with the collapse of the building, providing evidence that the methodology is effective in detecting vulnerable areas.

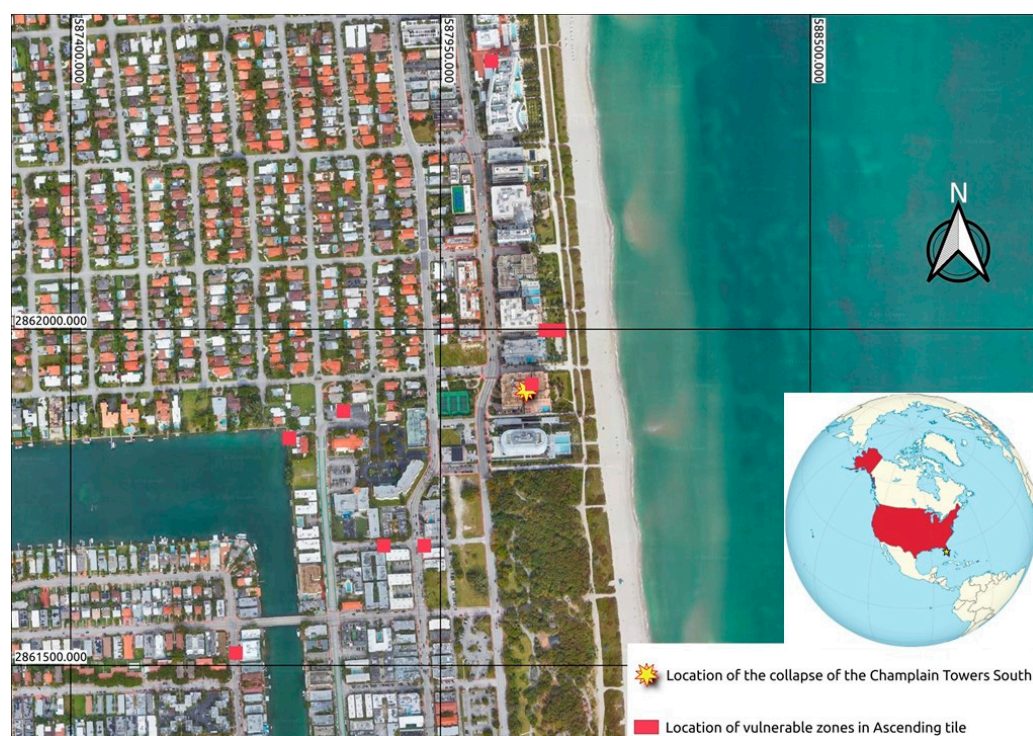


Figure 13. The vulnerable zone geographically concurs with the Champlain Towers South building, which partially collapsed.

Table 4 includes the results of the case studies, showing a potential excess of alerts in vulnerable zones and/or a lack of precision for the location of the collapse. These results exhibit the influence of temporal decorrelation caused by vegetation or the proximity to water areas, such as the case of Peñíscola. In order to address the inaccuracies in the results, this supplementary information about the surrounding areas of interest could be used to discard alerts in non-urbanized and vegetation areas.

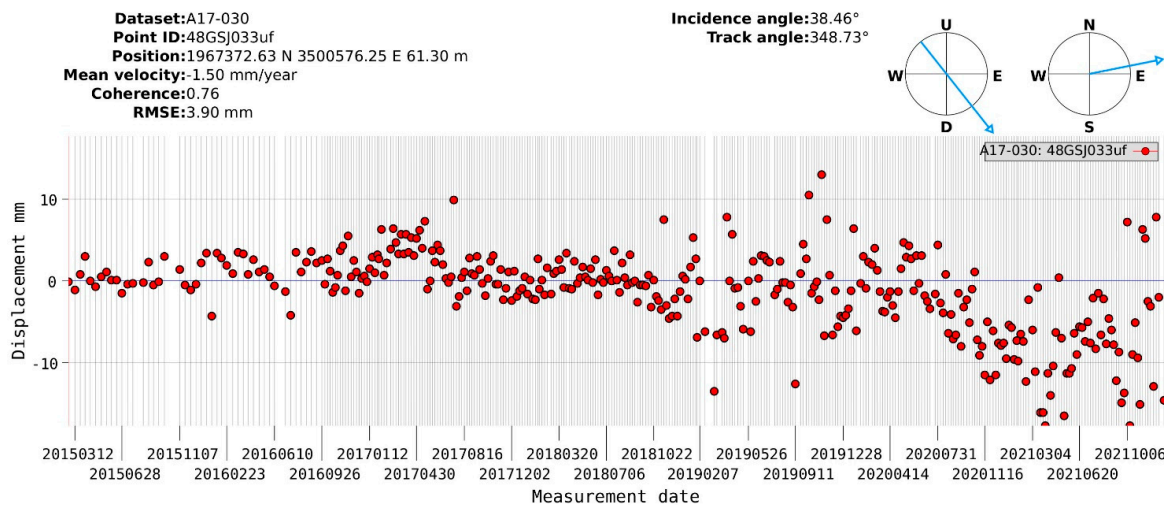
Table 4. Summary of the results of the four case studies analyzed.

Case Study	Number of Alert Pixels in Tile	Minimum Distance between the Actual Structure Collapse and the Nearest Collapse Risk Alert Pixel
Line 12 of the Mexico City Metro	9	$\cong 540$ m (concurr with one of the girders supporting the overpass carrying Line 12 of the Mexico City Metro near the Tezonco station)
Caprigliola bridge	9	$\cong 20$ m (in the streambed where the bridge collapsed)
Building in the Font Nova urbanization (Peñíscola)	30	$\cong 65$ m (coincides geographically with the environment of the collapsed building)
Miami	9	$\cong 0.50$ m (exact geographical overlay on the collapsed building)

We use the European Ground Motion Service (EGMS), which provides accurate and consistent information on natural and anthropogenic ground motion with millimeter precision [38], to compare our results of vulnerable zones in the European case studies. In the case study of the building in the Font Nova urbanization (Peñíscola), Figure 14 shows the difficulty of the early detection of infrastructure at risk in isolation due to the high variability of ground motion values. If we take the most extreme value, which coincides with the building that collapsed, we can see that it had an average ground motion velocity of -1.5 mm/year in ascending images and -1.7 in descending images; in fact, the trend graph presents an almost stable picture before the collapse on 25 August 2021, which suggests it is practically impossible to anticipate risks.



(a)



(b)



(c)

Figure 14. Cont.

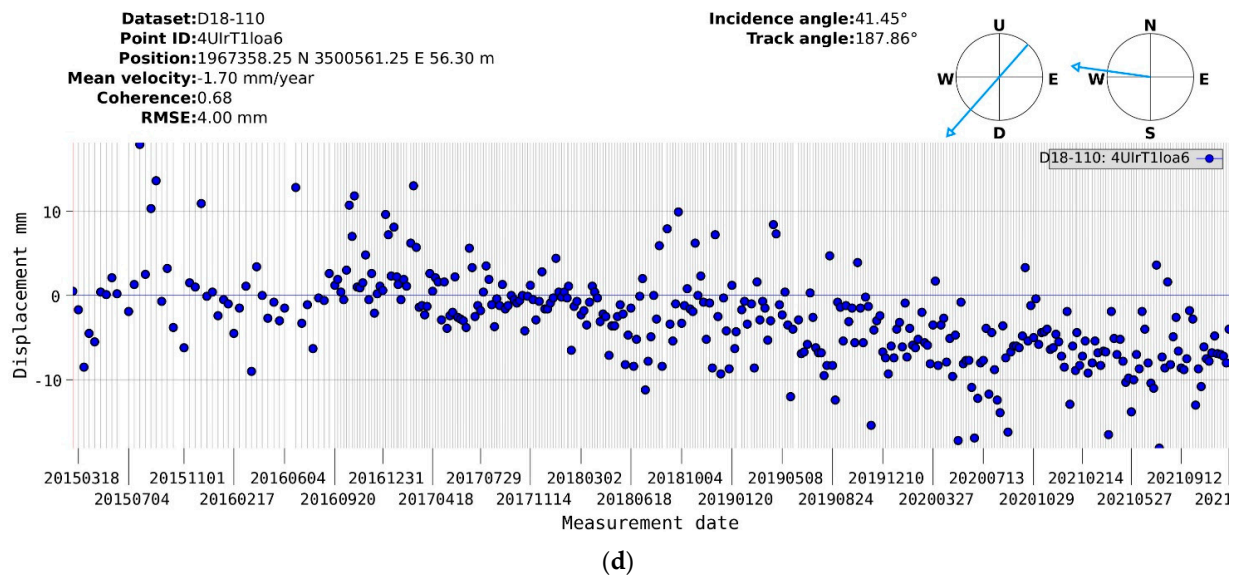


Figure 14. (a) Ground motion in the ascending track from EGMS [38] in the area of the building collapse in the Font Nova urbanization (Peñíscola). (b) Deformation time series in the ascending track of the point with the highest value of ground motion located in the building collapse. (c) Ground motion in the descending track from EGMS in the area of the Font Nova urbanization. (d) Deformation time series in the descending track of the point with the highest value of ground motion located in the building collapse.

In the case study of the Caprigliola bridge in Figure 15, the average ground motion velocity is -3.4 mm/year in ascending images and -2.7 in descending images. However, the trend graph shows stability before the collapse on 8 April 2020, and the trend graph changed only after the date of collapse, indicating the difficulty of anticipating the risks with this monitoring service.

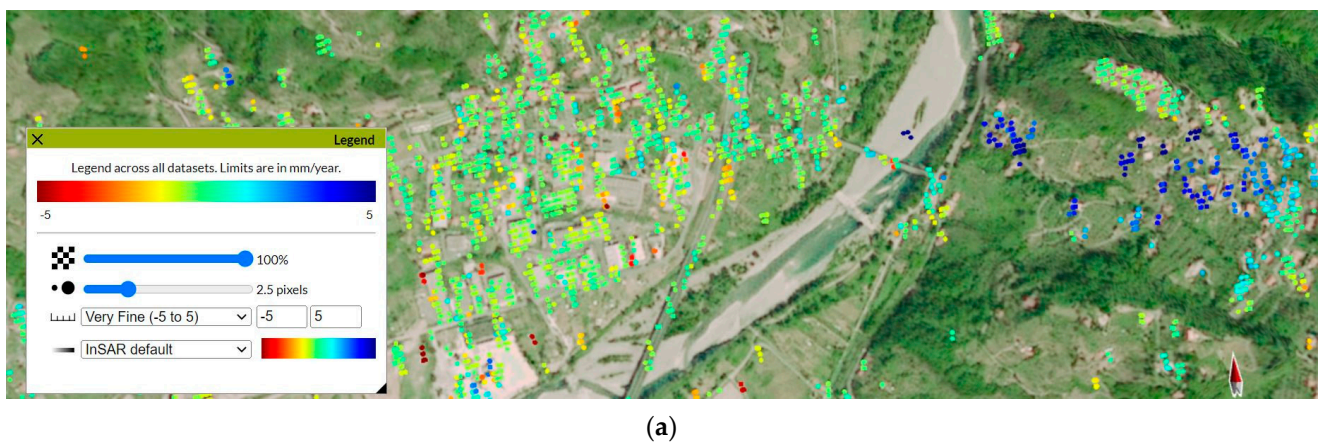
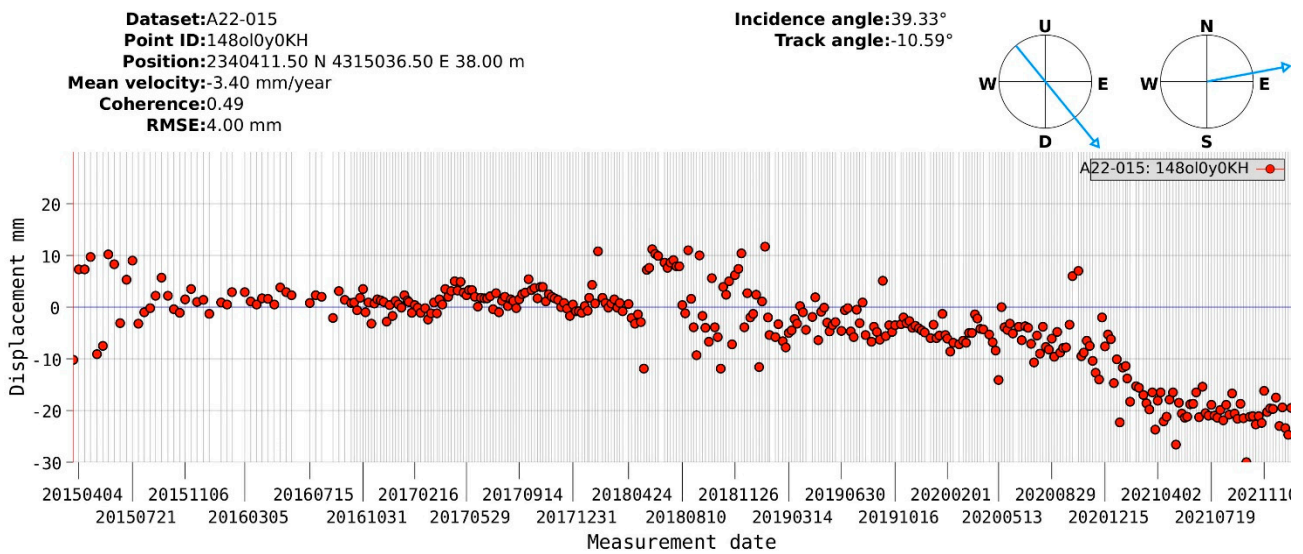


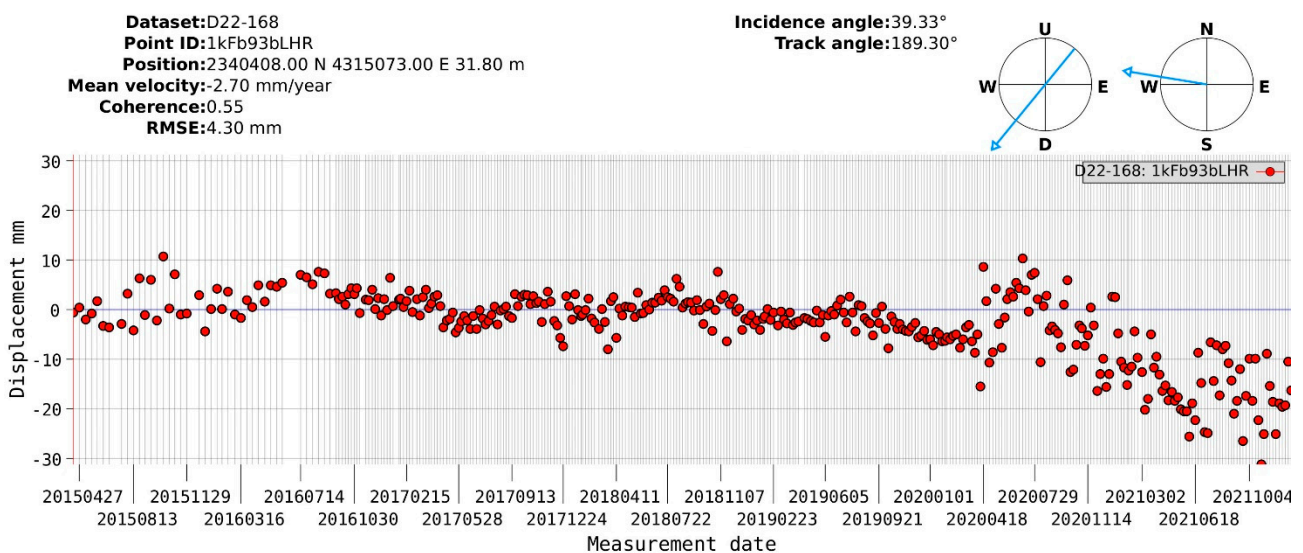
Figure 15. Cont.



(b)



(c)



(d)

Figure 15. (a) Ground motion in the ascending track from EGMS [38] in the area of the Capriogliola bridge collapse. (b) Deformation time series in the ascending track of the point with the highest value of ground motion located at the bridge collapse. (c) Ground motion in the descending track from EGMS around the Capriogliola bridge collapse. (d) Deformation time series in the descending track of the point with the highest value of ground motion located at the bridge collapse.

5. Discussion

In the Miami case study, the effectiveness of the 2σ -filter cutoff for both ascent and descent could not be verified due to the unavailability of descending images. Nevertheless, filtering the available data yielded satisfactory results, indicating the potential of our methodology to detect risks in areas with limited satellite image coverage. Our methodology provides a means to anticipate potential risk events by identifying areas close to actual collapses before they occur, allowing for immediate and direct identification of priority areas for in situ inspection, thereby optimizing human and financial resources in the evaluation of infrastructure globally.

In contrast to previous studies that analyzed internal trends [18–21] or common areas following the same trend pattern [22–26], our work evaluated known areas where a real infrastructure collapse occurred, demonstrating that our proposed methodology can detect vulnerabilities before the event occurs. This legitimizes the detection of vulnerable zones before they become a hazard.

One of the greatest advantages of our methodology is its accessibility and simplicity, as it requires only open images and programs (with the exception of MATLAB, which is necessary to execute the free StaMPS commands). Results for any case study can be obtained by following the manuals available online and applying only a few rules or filters. This replicability enables our methodology to be easily incorporated as an additional input to risk assessment procedures.

However, our methodology presents several challenges that must be addressed in the future. For example, the large amount of data required to compare registered displacements year by year makes computational performance more expensive. To overcome this, we suggest exploring the possibility of achieving comparable results with a single analysis (classical method) by dividing its trend directly by years. This would optimize the analysis, making it more restrictive in identifying vulnerable zones and reducing false alarms.

6. Conclusions

A methodology for the automated detection of vulnerable zones in the built environment, based on an annual comparison of the accumulated variation of the displacement trend, has been proposed. The detection of vulnerable areas is achieved using the MT-InSAR technique through radar satellite images (Sentinel-1), and has been tested in real-world scenarios.

The proposed methodology offers an accessible and cost-effective approach to monitoring infrastructure assets, aiming at preventing eventual structural collapses. The use of free and widely available radar images (Sentinel-1) and MT-InSAR technology, along with free software programs (SNAP, StaMPS, QGIS), makes this approach highly accessible.

By comparing displacement trends between pixels at the same geographical location over time, the methodology successfully detects potentially vulnerable zones, as demonstrated by four real cases of infrastructure collapse where the areas of potential risk were detected before the actual collapse occurred.

The simplicity of the methodology and its replicability make it a valuable tool for creating risk maps. This allows authorities to focus their attention on areas that require priority in situ inspection, leading to a rapid response in disaster prevention, reduction, and relief. Overall, this work offers a significant contribution to the field of infrastructure monitoring and provides a foundation for future research in this area.

As future work, we suggest also testing the decomposition of LOS displacement to obtain E-W and up-down displacement, which could locate areas with a stronger displacement trend. Finally, exploring the use of machine learning to discern potential false risks by incorporating other sources of information could be further explored for a more efficient and precise methodology that can rule out noise or false alerts in the results.

Author Contributions: Conceptualization, I.R.-A., J.M.-S. and B.R.; Methodology, I.R.-A.; Validation, M.C.; Writing—original draft, I.R.-A.; Writing—review & editing, J.M.-S., M.C. and B.R.; Supervision, J.M.-S. and B.R.; Funding acquisition, B.R. All authors have read and agreed to the published version of the manuscript.

Funding: This project has received funding from the European Union’s Horizon 2020 research and innovation program under grant agreement No. 958171. This work has been partially supported by the Spanish Ministry of Science and Innovation through the PONT3 project Ref. PID2021-124236OB-C33. This document reflects only the views of the authors. Neither the Innovation and Networks Executive Agency (INEA) nor the European Commission is in any way responsible for any use that may be made of the information it contains.

Conflicts of Interest: The authors declare no conflict of interest.

References

- Enrico, A.; Grosso, D.; Del Grosso, A.E. Structural Health Monitoring: Research and Practice. Structural Health Monitoring, Lifecycle and BIM View Project Parametric Design, Form Finding and Optimisation of Shell, Gridshell and Spatial Structures View Project Structural Health Monitoring: Research and Practice. 2013. Available online: <https://www.researchgate.net/publication/261119109> (accessed on 13 February 2023).
- Moreu, F.; Li, X.; Li, S.; Zhang, D. Technical specifications of structural health monitoring for highway bridges: New chinese structural health monitoring code. *Front. Built Environ.* **2018**, *4*, 10. [CrossRef]
- Kaneko, S.; Toyota, T. Long-term urbanization and land subsidence in Asian megacities: An indicators system approach. In *Groundwater and Subsurface Environments: Human Impacts in Asian Coastal Cities*; Springer: Berlin/Heidelberg, Germany, 2011; pp. 249–270. [CrossRef]
- Wang, H.M.; Wang, Y.; Jiao, X.; Qian, G.R. Risk management of land subsidence in Shanghai. *Desalination Water Treat.* **2014**, *52*, 1122–1129. [CrossRef]
- Solarski, M.; Machowski, R.; Rzetala, M.; Rzetala, M.A. Hypsometric changes in urban areas resulting from multiple years of mining activity. *Sci. Rep.* **2022**, *12*, 2982. [CrossRef]
- Xue, F.; Lv, X.; Dou, F.; Yun, Y. A Review of Time-Series Interferometric SAR Techniques: A Tutorial for Surface Deformation Analysis. Institute of Electrical and Electronics Engineers Inc. *IEEE Geosci. Remote Sens. Mag.* **2020**, *8*, 22–42. [CrossRef]
- Nádudvari, Á. Using radar interferometry and SBAS technique to detect surface subsidence relating to coal mining in Upper Silesia from 1993–2000 and 2003–2010. *Environ. Socio-Econ. Stud.* **2016**, *4*, 24–34. [CrossRef]
- Przylucka, M.; Herrera, G.; Graniczny, M.; Colombo, D.; Béjar-Pizarro, M. Combination of Conventional and Advanced DInSAR to Monitor Very Fast Mining Subsidence with TerraSAR-X Data: Bytom City (Poland). *Remote Sens.* **2015**, *7*, 5300–5328. [CrossRef]
- MacChiarulo, V.; Milillo, P.; Blenkinsopp, C.; Reale, C.; Giardina, G. Multi-temporal InSAR for transport infrastructure monitoring: Recent trends and challenges. *Proc. Inst. Civ. Eng. Bridge Eng.* **2021**, *176*, 92–117. [CrossRef]
- Malik, K.; Kumar, D.; Perissin, D.; Pradhan, B. Estimation of ground subsidence of New Delhi, India using PS-InSAR technique and Multi-sensor Radar data. *Adv. Space Res.* **2022**, *69*, 1863–1882. [CrossRef]
- Chang, L.; Dollevoet, R.P.B.J.; Hanssen, R.F. Monitoring Line-Infrastructure with Multisensor SAR Interferometry: Products and Performance Assessment Metrics. *IEEE J. Sel. Top. Appl. Earth Obs. Remote Sens.* **2018**, *11*, 1593–1605. [CrossRef]
- Free and Open Source Software (FOSS). Available online: <https://en.unesco.org/freeandopensourcesoftware> (accessed on 3 January 2022).
- Ferretti, A.; Prati, C.; Rocca, F. Nonlinear subsidence rate estimation using permanent scatterers in differential SAR interferometry. *IEEE Trans. Geosci. Remote Sens.* **2000**, *38*, 2202–2212. [CrossRef]
- Blasco, J.D.; Foulmelis, M.; Stewart, C.; Hooper, A. Measuring Urban Subsidence in the Rome Metropolitan Area (Italy) with Sentinel-1 SNAP-StaMPS Persistent Scatterer Interferometry. *Remote Sens.* **2019**, *11*, 129. [CrossRef]
- Bakon, M.; Perissin, D.; Lazecky, M.; Papco, J. Infrastructure Non-linear Deformation Monitoring via Satellite Radar Interferometry. *Procedia Technol.* **2014**, *16*, 294–300. [CrossRef]
- Chang, L.; Dollevoet, R.P.B.J.; Hanssen, R.F. Nationwide Railway Monitoring Using Satellite SAR Interferometry. *IEEE J. Sel. Top. Appl. Earth Obs. Remote Sens.* **2017**, *10*, 596–604. [CrossRef]
- Sousa, J.J.; Bastos, L. Multi-temporal SAR interferometry reveals acceleration of bridge sinking before collapse. *Nat. Hazards Earth Syst. Sci.* **2013**, *13*, 659–667. [CrossRef]
- Bischoff, C.A.; Ferretti, A.; Novali, F.; Uttini, A.; Giannico, C.; Meloni, F. Nationwide deformation monitoring with SqueeSAR[®] using Sentinel-1 data. *Proc. Int. Assoc. Hydrol. Sci.* **2020**, *382*, 31–37. [CrossRef]
- Raspini, F.; Bianchini, S.; Ciampalini, A.; Del Soldato, M.; Montalti, R.; Solari, L.; Tofani, V.; Casagli, N. Persistent Scatterers continuous streaming for landslide monitoring and mapping: The case of the Tuscany region (Italy). *Landslides* **2019**, *16*, 2033–2044. [CrossRef]
- Raspini, F.; Bianchini, S.; Ciampalini, A.; Del Soldato, M.; Solari, L.; Novali, F.; Del Conte, S.; Rucci, A.; Ferretti, A.; Casagli, N. Continuous, semi-automatic monitoring of ground deformation using Sentinel-1 satellites. *Sci. Rep.* **2018**, *8*, 7253. [CrossRef] [PubMed]

21. Del Soldato, M.; Solari, L.; Raspini, F.; Bianchini, S.; Ciampalini, A.; Montalti, R.; Ferretti, A.; Pellegrineschi, V.; Casagli, N. Monitoring Ground Instabilities Using SAR Satellite Data: A Practical Approach. *ISPRS Int. J. Geo-Inf.* **2019**, *8*, 307. [[CrossRef](#)]
22. Zhu, M.; Wan, X.; Fei, B.; Qiao, Z.; Ge, C.; Minati, F.; Vecchioli, F.; Li, J.; Costantini, M. Detection of Building and Infrastructure Instabilities by Automatic Spatiotemporal Analysis of Satellite SAR Interferometry Measurements. *Remote Sens.* **2018**, *10*, 1816. [[CrossRef](#)]
23. Barra, A.; Solari, L.; Béjar-Pizarro, M.; Monserrat, O.; Bianchini, S.; Herrera, G.; Crosetto, M.; Sarro, R.; González-Alonso, E.; Mateos, R.M.; et al. A Methodology to Detect and Update Active Deformation Areas Based on Sentinel-1 SAR Images. *Remote Sens.* **2017**, *9*, 1002. [[CrossRef](#)]
24. Luo, S.; Feng, G.; Xiong, Z.; Wang, H.; Zhao, Y.; Li, K.; Deng, K.; Wang, Y. An Improved Method for Automatic Identification and Assessment of Potential Geohazards Based on MT-InSAR Measurements. *Remote Sens.* **2021**, *13*, 3490. [[CrossRef](#)]
25. Tomás, R.; Pagán, J.I.; Navarro, J.A.; Cano, M.; Pastor, J.L.; Riquelme, A.; Cuevas-González, M.; Crosetto, M.; Barra, A.; Monserrat, O.; et al. Semi-Automatic Identification and Pre-Screening of Geological–Geotechnical Deformational Processes Using Persistent Scatterer Interferometry Datasets. *Remote Sens.* **2019**, *11*, 1675. [[CrossRef](#)]
26. Bianchini, S.; Solari, L.; Casagli, N.; Tomás, R.; Löw, F.; Thenkabail, P.S. A GIS-Based Procedure for Landslide Intensity Evaluation and Specific risk Analysis Supported by Persistent Scatterers Interferometry (PSI). *Remote Sens.* **2017**, *9*, 1093. [[CrossRef](#)]
27. SNAP—STEP. Available online: <http://step.esa.int/main/toolboxes/snap/> (accessed on 4 January 2021).
28. Blasco, J.M.D.; Fomelis, M. Automated SNAP Sentinel-1 DInSAR Processing for StaMPS PSI with Open Source Tools. In Proceedings of the International Geoscience and Remote Sensing Symposium 2018 (IGARSS 2018), Valencia, Spain, 22–27 July 2018. [[CrossRef](#)]
29. GitHub-dbekaert/StaMPS: Stanford Method for Persistent Scatterers. Available online: <https://github.com/dbekaert/stamps> (accessed on 16 January 2023).
30. StaMPS/2-4_StaMPS-steps.md Master Matthias/gis-Blog GitLab. Available online: https://gitlab.com/Rexthor/gis-blog/-/blob/master/StaMPS/2-4_StaMPS-steps.md (accessed on 10 February 2021).
31. Por Qué Colapsó la Línea 12 del Metro de Ciudad de México—The New York Times. Available online: <https://www.nytimes.com/es/interactive/2021/06/12/espanol/america-latina/metro-ciudad-de-mexico.html> (accessed on 3 January 2022).
32. È Crollato un Ponte su una Strada Provinciale tra Toscana e Liguria—Il Post. Available online: <https://www.ilpost.it/2020/04/08/crollo-ponte-liguria-toscana-aulla-bolano/> (accessed on 3 January 2022).
33. Semana Clave para Conocer las Causas del Derrumbe en Peñíscola que Costó la Vida a dos Personas | Radio Valencia | Cadena SER. Available online: https://cadenaser.com/emisora/2021/09/25/radio_valencia/1632567036_278947.html (accessed on 3 January 2022).
34. Why Did This Florida Condo Building Collapse? Experts Explain. The New York Times. Available online: <https://www.nytimes.com/2021/06/27/us/miami-building-investigation-clues.html> (accessed on 3 January 2022).
35. Corruption in North Miami Beach Could Be Factor in Surfside Building Collapse: 7 Things to Know. Available online: <https://moguldom.com/362247/corruption-in-north-miami-beach-could-be-factor-in-surfside-building-collapse-7-things-to-know/> (accessed on 3 January 2022).
36. Surfside Condo Built in Era Tainted by Corruption | Fred Grimm—South Florida Sun Sentinel—South Florida Sun-Sentinel. Available online: <https://web.archive.org/web/20210714183615/https://www.sun-sentinel.com/opinion/commentary/fl-op-com-grimm-south-florida-building-inspectors-corruption-20210702-6u6kamfs4vcefatc6iqbidns6y-story.html> (accessed on 3 January 2022).
37. Surfside Condo Collapse Is Third Largest Building Failure in Country’s History—CBS Miami. Available online: <https://miami.cbslocal.com/2021/06/29/surfside-condo-collapse-third-largest-building-failure-us-history/> (accessed on 3 January 2022).
38. European Ground Motion Service—Copernicus Land Monitoring Service. Available online: <https://land.copernicus.eu/pan-european/european-ground-motion-service> (accessed on 20 January 2023).

Disclaimer/Publisher’s Note: The statements, opinions and data contained in all publications are solely those of the individual author(s) and contributor(s) and not of MDPI and/or the editor(s). MDPI and/or the editor(s) disclaim responsibility for any injury to people or property resulting from any ideas, methods, instructions or products referred to in the content.